Matching fixed order Matrix Elements to Parton Showers for heavy quark production in e^+e^- annihilation

Carlos Ortiz*
Thesis for Master of Science degree
Department of Theoretical Physics, Lund University
Sölvegatan 14A, S-22362 Lund, Sweden

May 7, 2002

Abstract

Multi-parton production can be described by fixed order *matrix elements* and/or *parton showers*. These are accurate in different and complementary regions of the available phase space. Matrix elements give a good description of the production of a few, widely separated partons, whereas parton showers are best suited to model the emission of many partons in the soft and collinear regions.
A combined treatment, where matrix elements are used together with the parton shower of the Colour-Dipole Cascade Model, is studied in the ARIADNE event generator, with emphasis on gluon radiation off *primary* heavy quarks and perturbative production of *secondary* heavy quark-antiquark pairs, $g \to Q\bar{Q}$.

Contents

*carlos@thep.lu.se

quarks	u up	c charm	t top
quarks	d down	s strange	b bottom
leptons	ν_e e-neutrino	ν_μ μ-neutrino	$'nu_\tau$ τ-neutrino
leptons	e electron	μ muon	τ tau
generation	I	II	III

INTERACTION	GRAVITY	WEAK	ELECTROMAGNETIC	STRONG
Carried by	Graviton (Not yet observed)	W^+, W^-, Z^0	Photon	Gluon
Acts on	All	Quarks, leptons, W^+, W^-, Z^0	Quarks, charged leptons, W^+, W^-	Quarks, gluons

Figure 1: **Up:** All leptons and quarks carry electrical charge, except for the neutrinos which are neutral. Quarks additionally have a degree of freedom in colour charge (e.g. red, blue, green). For each particle there exists an oppositely charged antiparticle. **Down:** Interactions are mediated by bosons. Gluons mediate the strong interaction and carry two degrees of freedom in colour.

1 Introduction

In an attempt to understand the behavior of nature, physicists have arrived at a theory of *elementary particles* and their *interactions*, together thought to be responsible for the formation of more complex structures (e.g. hadrons, atoms, molecules, etc.). Building blocks of this theory today are leptons, quarks, gauge bosons and the Higgs boson[1] (see **figure 1**).

Quantum Field Theory (QFT) provides the theoretical framework for the electroweak and the strong interaction, which together comprise the *Standard Model* of particle physics. Quantum Chromodynamics (QCD) describes the strong interaction.

No satisfactory theory embedding both gravitation and Quantum Mechanics exists yet. Since the energies available for conducting experiments on elementary particles today are of order 10^2-10^3 GeV, and since gravitational interactions can be considered negligible at particle energies of these orders of magnitude, we will not treat gravity in what follows.

Not all features of the Standard Model have been satisfactorily understood yet. In order to explore and to increase our comprehension of the structure of nature, facilities have been developed to conduct experiments of interest. Relevant to this work are colliders used to perform experiments on strongly interacting particles, quarks and gluons, commonly called *partons*[2].

No free quarks have ever been directly observed at the experiments, but indirect indications on the partonic structure of matter, have been concluded from observations made of more than two hundred of their bound states, commonly called *hadrons*.

While attempting to understand what takes place and leads to the observations recorded at experiments, information is gained on processes not well described by the fundamental QCD theory. Conclusions from experimental results and theoretical modelling have been

[1] Couples to mass, not yet observed.

[2] Quarks are charged with one colour. Gluons are charged with one colour and one anticolour simultaneously.

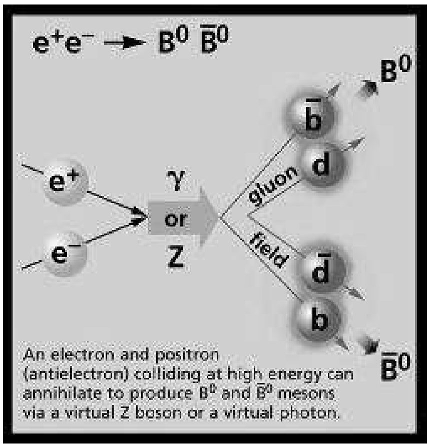

Figure 2: Illustration of the creation of a primary bottom-antibottom pair, giving rise to a colour field, from which secondary quark-antiquark pairs are created, for simplicity we here choose to only illustrate one of these.

implemented in computer programs, *event generators*[1, 2, 3], which attempt to reproduce the physics relevant for producing partons and forming the observed hadrons.

In event generators, *all* processes of interest need to be simultaneously considered at *all* stages of the evolution, in order to make accurate predictions for the observations made at the detectors. When known to accurately reproduce well established results, event generators can be used as an analysing tool, and to anticipate what might be observed when exploring *new features* at experiments being designed and proposed.

For a more elaborate introduction to modern particle physics we refer the reader to [4, 5, 6, 7]. Here, we will specifically study the reproduction of processes related to the decays of photons or Z^0-bosons into a *primary* quark-antiquark pair, $q\bar{q}$, which subsequently enters a QCD *cascade*; i.e. radiates gluons and creates new *secondary* quark-antiquark pairs, $Q\bar{Q}$ (see **figure 2**).

At a later stage of the evolution, all parton created will fuse into hadrons, i.e. quark-antiquark bound states called *mesons* and bound states of three quarks or antiquarks called *baryons*. At the detectors, observations will be made as *showers* of hadrons[3] distributed within narrow *jets* in phase-space.

The production of new partons in the QCD cascade is today well described by *parton shower* algorithms implemented in event generators. Together with fragmentation models [8, 9] for the transition of partons into hadrons, most results obtained e.g. at the LEP accelerator at CERN are reproduced, although discrepancies are found when working with many *widely separated* jets [10] and *massive* quarks [11].

The current work is based on the ideas presented in [12], where the Colour-Dipole Cascade Model (CDM) [13, 14], as implemented in the ARIADNE [1] event generator, was matched to exact tree-level matrix elements for $e^+e^- \to n$-parton processes. Here we will be specifically interested in the properties of massive or *heavy* quarks when generated by this new treatment.

Although quark masses remain not very precisely constrained, they impose a restriction on which flavours might be kinematically available for production. For this study in particular, carried out at LEP energies, $t\bar{t}$-pairs would be too massive to be created at any stage

[3]Colour neutral combinations, i.e. red-antired or red-green-blue

of the evolution, ($E_{CM,LEP} \approx m_{Z^0} \approx \frac{1}{2}m_t$), and are therefore excluded from this study.

The outline of this work will be the following:
In **chapter 2** we make an brief presentation of necessary concepts from QCD. In sections **2.1-2.2**, we discuss the production of partons through matrix elements and parton showers respectively. In section **2.3** the CDM is presented, and in section **2.4** jet clustering algorithms are discussed.
Chapter 3 treats the features of a combined approach between matrix elements and the CDM. In **chapter 4** some results are presented and finally in **chapter 5** some conclusions are drawn.

2 Quantum Chromodynamics, QCD

The uncertainty principle from Quantum Mechanics bounds the distance over which an interaction takes place to the *momentum transfer* or *scale* at stake, $\Delta x \Delta p \sim 1$. What contributes to an interaction at some scale, Q, is then bounded in resolution by $\Delta x \sim \frac{1}{Q}$.
The coupling of fields in QCD is a *function* of the momentum transfer, to lowest order[4] it is given by

$$\alpha_s(Q^2) = \frac{12\pi}{(11N_c - 2n_f)\log{(Q^2/\Lambda^2)}}. \tag{1}$$

The additional quantities N_c, n_f, Λ are the number of colour charges (=3), the number of *available* quark flavours (=5) and the fundamental QCD scale parameter ($\sim 200MeV$) respectively.

Two interesting features encountered in QCD are:

- **Asymptotic freedom**
  From eq. (1) we conclude that the coupling of fields decreases when the scale increases. At high enough scales the QCD coupling becomes sufficiently small for quarks and gluons to behave as free particles.
- **Confinement**
  The energy stored in a colour field between partons *increases* proportional to the distance, it eventually becomes favourable to create new partons from the field rather than to further increase their separation.

In event generators, the evolution can be divided into two regimes:

1. At scales greater than approximately $1\,GeV$, the strong coupling is in the *perturbative* regime, i.e. the predictions of an observable involving strong interactions can be expanded in a power series of the coupling.
2. At scales smaller than $1\,GeV$, the strong coupling is large and power expansions are no longer applicable. No satisfactory dynamic description of this *non-perturbative* regime, derived from basic theoretical principles such as the QCD Lagrangian, has yet been presented.

Once a primary $q\bar{q}$-pair is created, it undergoes a perturbative parton cascade, which for this study is modelled by the CDM in Ariadne, down to scales where non-perturbative processes grow significant and become responsible for the formation of hadrons.

Phenomenological models for the transition from partons to hadrons are needed. The ones

[4]In field theory one keeps track of contributions to a given order. The higher the order we go to, the more terms we need to simultaneously consider.

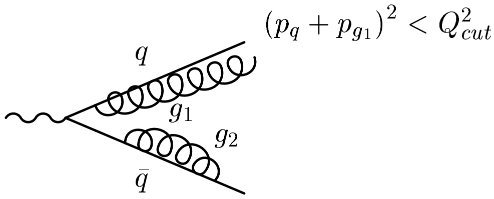

Figure 3: Matrix elements diverge for soft and collinear partons. These divergences are regulated by a cutoff in resolution, e.g. excluding configurations where $(p_q + p_{g_1})^2 < Q^2_{cut}$.

available [8, 9] need the *soft* and *collinear* regions[5] to be properly described, as it is done by the parton showers but poorly accomplished by fixed order matrix elements.

Matrix element calculations are *exact* to a given order, and hence give a good description of a few energetic widely separated partons, whereas the accuracy in parton shower models is limited to the soft and collinear regions.

Energetic or *hard* emissions significantly alter the jet-structures of events; furthermore, apart from the heavy flavours produced at the $\gamma^*/Z^0 \to q\bar{q}$ decays, c and b quarks are only expected to be produced by the perturbative splitting of energetic gluons, $g \to Q\bar{Q}$.

Events with several widely separated jets involving heavy quarks are important signals for the Higgs-boson production, and most other exotic particle searches. It is therefore desirable to be able to properly describe backgrounds to these processes from ordinary QCD events.

Our aim is to improve the CDM in ARIADNE, with respect to the reproduction of hard gluon emissions and secondary quark-antiquark pair production, and in particular to study the differences on heavy quarks when generated by this new approach.

Although hadronization needs to be added to the parton-level results before confronting predictions with experimental observations, we will in this study only be interested in the qualitative differences between the partons produced by the matrix element corrected- and the standard CDM. We will present results at the bare parton-level, where the final *jet-topologies* for widely separated jets should not be altered significantly by non-perturbative processes. Suitably defined, the energies and directions of these jets directly reflect the energies and directions of the partons produced at the decays.

2.1 Matrix elements for $e^+e^- \to n$-partons

In QFT, the transition probabilities between states are given by the matrix elements, which can be derived through Feynman diagrams. To some given order in α_s, the transition matrices for $e^+e^- \longrightarrow n$ partons are derived from all n-parton final state diagrams allowed.

We make a distinction between *real* (tree-level) diagrams and *virtual* (containing *loops*) diagrams. Loops are drawn as closed internal lines, so that virtual n-parton diagrams are of higher order in α_s, i.e. include more QCD vertices, than real n-parton ones.

The *cross sections* for given $e^+e^- \to n$-parton configurations, are obtained when integrating the transition amplitudes squared over the states available in phase space

$$\sigma_{i\to f} = \frac{1}{2\left(\sum_i p_i\right)^2} \int |\mathcal{M}_{i\to f}|^2 \, d\Omega_{i\to f} \qquad (2)$$

For soft and collinear partons the matrix elements diverge, even though α_s might be small, and the perturbative expansion breaks down, therefore when making calculations there is a

[5]**Soft** partons carry low energy fractions. **Collinear** partons are emitted with small opening angle.

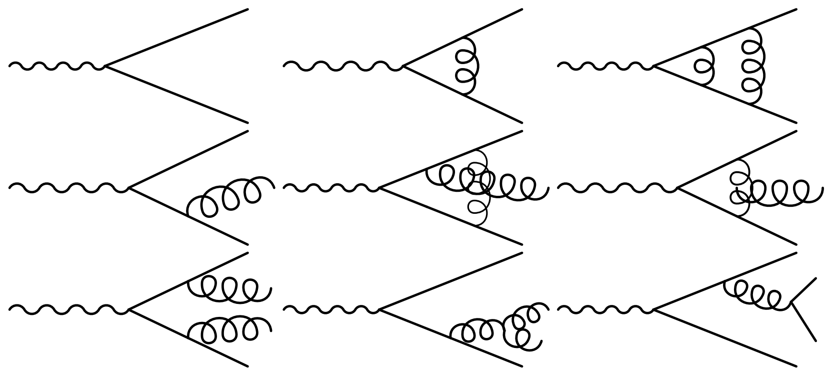

Figure 4: Some matrix elements to order α_s^2 contributing to $\gamma^*/Z^0 \to 2,3,4$-partons processes.

need to introduce a cutoff scale in resolution, Q^2_{cut}, sufficiently high to exclude the regions of phase space where the matrix elements diverge (see **figure 3**).

For this work we will use matrix elements to order α_s^2. Some of the relevant diagrams are shown in **figure 4**, grouped according to how they contribute to the probabilities for n resolved[6] partons.

Having introduced this cutoff and the centre-of-mass energy for the collision, Q^2, we can write the probability fractions for *n-jet* events, $R_n\left(Q^2, Q^2_{cut}\right)$, as

$$\begin{aligned} R_2(Q^2,Q^2_{cut}) &= 1 + \alpha_s C_{0,1}(Q^2,Q^2_{cut}) + \alpha_s^2 C_{0,2}(Q^2,Q^2_{cut}) \\ R_3(Q^2,Q^2_{cut}) &= \alpha_s C_{1,1}(Q^2,Q^2_{cut})\left[1 + \alpha_s C_{1,2}(Q^2,Q^2_{cut})\right] \\ R_4(Q^2,Q^2_{cut}) &= \alpha_s^2 C_{2,2}(Q^2,Q^2_{cut}), \end{aligned} \tag{3}$$

with all resolved $\mathcal{O}\left(\alpha_s^m\right)$ contributions to $(n+2)$-parton final states symbolically collected in the coefficients, $C_{n,m}\left(Q^2, Q^2_{cut}\right)$, i.e. $C_{n,n}$ contains tree-level diagrams and $C_{n,m}$, with $m > n$, contains the sum of virtual and unresolved diagrams.

Virtual and unresolved contributions diverge separately, but their sum is finite. We redefine the *virtual corrections* as being the usual virtual diagrams together with unresolved diagrams.

The cutoff, Q^2_{cut}, then acts as a limit on *closeness* among final state partons from matrix element calculations. The lower the cutoff is chosen to be, the more of the divergent structure from the logarithms of $\frac{Q^2}{Q^2_{cut}}$ inherent in the $C_{n,m}$ terms[7] we are including, and the more detailed jet structures we are considering. If Q^2_{cut} is chosen too small the whole expansion is destroyed.

Working out the actual tree-level matrix elements for n-parton final states becomes a difficult computational task as n increases. Considering interference, the number of terms in $|\mathcal{M}_{i\to f}|^2$ grows significantly[8] with n, furthermore, when working with massive quarks, restrictions to the phase space complicate the integration in eq. (2), e.g. the propagators for quark lines pick up poles at $p_q^2 = m_q^2$. Presently, complete calculations have been presented up to order α_s^2 in [15].

For $|\mathcal{M}_{\gamma^*/Z^0 \to\, qg\bar{q}}|^2$ particularly, the contributing diagrams are illustrated in **figure 5**.

[6]Diagrams with no emissions below Q^2_{cut}, i.e. n-jet processes with respect to this resolution.
[7]See evolution equation (6).
[8]For each flavour there are 3 combinations for the $q\bar{q}$ final state, 10 for the $qg\bar{q}$, 76 for the $q\bar{q}gg$, 554 for the $q\bar{q}q\bar{q}$ and 528 for the two flavour combination $q\bar{q}q'\bar{q}'$

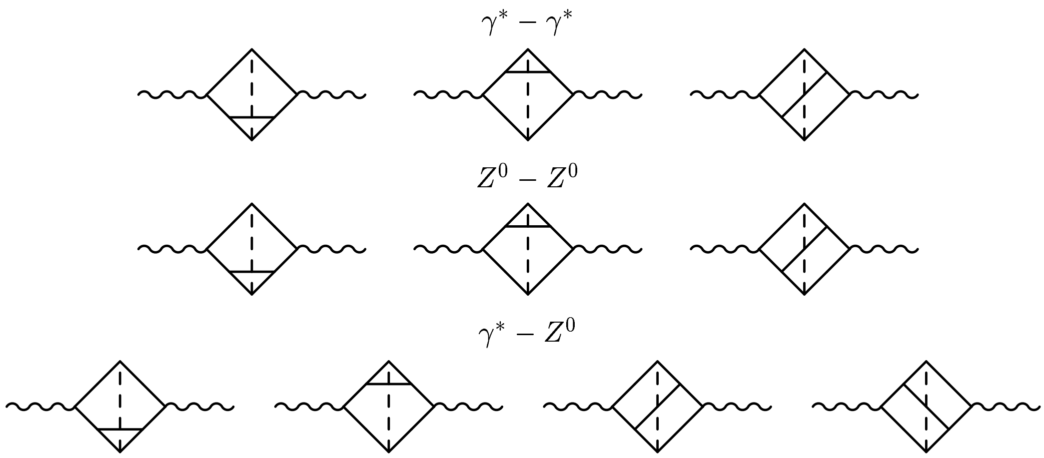

Figure 5: Squared amplitude diagrams contributing to $|\mathcal{M}_{\gamma^*/Z^0 \to\, qg\bar{q}}|^2$. For the γ^*-Z^0 interference there is an additional term, corresponding to an extra configuration possible for the emission of the gluon, i.e. either emitted between a quark from a γ^* decay and an antiquark from a Z^0 decay, or between an antiquark from a γ^* decay and a quark from a Z^0 decay.

2.2 Parton showers

Many-parton matrix elements are dominated by configurations where the gluons are emitted at widely different scales, so that the real matrix elements as well as the virtual contributions factorize[9], e.g. for n *soft* gluons radiating from either the quark or the antiquark, the matrix elements obtain the exponential structure [16]

$$|\mathcal{M}_{qg^n\bar{q}}|^2 \sim \frac{\alpha_s^n}{n!}\left(\prod_{i=1}^{n}\frac{2p_1p_2}{(p_1k_i)\,(p_2k_i)}\right)|\mathcal{M}_{q\bar{q}}|^2 \tag{4}$$

where k_i are the gluon momenta, p_1 and p_2 are the quark and antiquark four-momenta, and the gluon self coupling neglected.

In the Leading Log Approximation (LLA) one only keeps track of perturbative contributions to the evolution equations where α_s is accompanied by large logarithms of Q^2, and neglects other *sub-leading*[10] terms. The expansion is performed to *all* orders keeping only contributions satisfying

$$\left[\alpha_s(Q^2)\cdot\log^2\left(Q^2\right)\right]^n \sim 1. \tag{5}$$

Thus, instead of truncating the perturbative expansion at a fixed power of α_s, we resum to infinite order, neglect sub-leading contributions, and obtain a finite answer. In the asymptotic limit, $Q^2 \to \infty$, the LLA becomes exact.

Parton shower models are based on this leading logarithmic expansion. Here the $q\bar{q}$-pair produced at the electroweak vertex enters the QCD cascade, emissions are approximated by factorising expression, and subsequently generated with respect to a set of branching probabilities, ordered in some variable of emission.

In Ariadne, the ordering is performed in decreasing *transverse momentum*, eq. (13), so that subsequent emissions always are emitted with smaller values than preceding ones.
Other ordering variables used are invariant mass in Pythia and angular ordering in Herwig.

[9] In a logarithmic sense, the emissions can be considered to be generated in different, well separated regions, and the overall probability to reach a specific configuration can be written as a product of all intermediate decays.

[10] $\alpha_s^n\left(Q^2\right)\cdot\log^m\left(Q^2\right)$ with $m < 2n$.

2.2.1 Branching probabilities

At high scales, the differential splitting probabilities for partons, $a \to b\,c$, are given by the Altarelli-Parisi evolution equations [17]

$$d\mathcal{P}_{a\to bc}(Q_a^2, z) = \frac{\alpha_s(Q_a^2)}{2\pi} P_{a\to bc}(z) \frac{dQ_a^2}{Q_a^2} dz, \tag{6}$$

with splitting functions

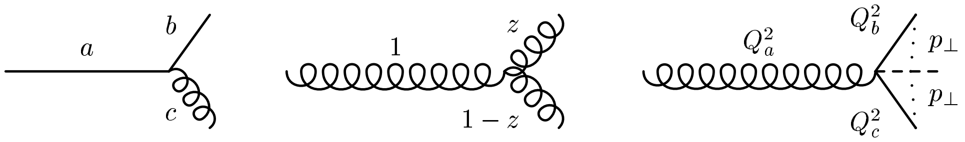

$$P_{q\to qg}(z) = \frac{4}{3}\frac{1+z^2}{1-z} \qquad P_{g\to gg}(z) = 3\frac{(1-z(1-z))^2}{z(1-z)} \qquad P_{g\to q\bar{q}}(z) = \frac{n_f}{2}(z^2 + (1-z)^2). \tag{7}$$

The z variable describes the distribution of energy between the daughters, parton b carrying an energy fraction z and parton c the remaining $(1-z)$. The boundaries of z will be given by some scale of emission, e.g. invariant mass $z_{min} \approx \frac{Q_b^2}{Q_a^2}$ or transverse momenta, $z_{min} \approx \frac{p_\perp^2}{Q_a^2}$.

Integrating eq. (6) with respect to z we obtain the *branching probabilities*, $\Gamma\left(\rho^2, Q^2\right)$. We will use the notations Γ_q, Γ_g, and Γ_f, for respective $q \to qg$, $g \to gg$, and $g \to q\bar{q}$ branchings, and let ρ^2 denote the ordering variable. These branching probabilities are given as

$$\begin{aligned}
\Gamma_q\left(\rho^2, Q^2\right) &= \frac{4}{3\pi}\frac{\alpha_s(\rho^2)}{\rho^2}\left(\ln\frac{Q^2}{\rho^2} - \frac{3}{4}\right) \\
\Gamma_g\left(\rho^2, Q^2\right) &= \frac{3}{\pi}\frac{\alpha_s(\rho^2)}{\rho^2}\left(\ln\frac{Q^2}{\rho^2} - \frac{11}{12}\right) \\
\Gamma_f\left(\rho^2\right) &= \frac{n_f}{6\pi}\frac{\alpha_s(\rho^2)}{\rho^2}.
\end{aligned} \tag{8}$$

i.e. the probability that a parton created at some arbitrary scale Q^2 will split at ρ^2.

2.2.2 Sudakov form factors

The Sudakov form factor [18], Δ_i, corresponds to the probability for parton i to evolve, without any resolvable branchings, in a given region of phase space. Its expansion in powers of α_s reveals its correspondence to the leading logarithmic approximation of the virtual corrections in eq. (3).

- For a quark or antiquark to evolve from Q to Q_0 without resolvable branchings one obtains a probability

$$\Delta_q(Q^2, Q_0^2) = \exp\left\{-\int_{Q_0^2}^{Q^2} \Gamma_q\left(\rho^2, Q^2\right) d\rho^2\right\}. \tag{9}$$

- For a gluon to evolve from Q to Q_0 without resolvable branchings one obtains a probability

$$\Delta_g(Q^2, Q_0^2) = \exp\left\{-\int_{Q_0^2}^{Q^2} \left[\Gamma_g\left(\rho^2, Q^2\right) + \Gamma_f(\rho^2)\right] d\rho^2\right\}. \tag{10}$$

In general, the structure of a Sudakov form factor, corresponding to reaching a n-parton state in the evolution, can be written as

$$\boldsymbol{\Delta}_{S_n}\left(Q^2, \ldots, Q_0^2\right) \approx \prod_i \Delta_i\left(\rho_i^2\right) \tag{11}$$

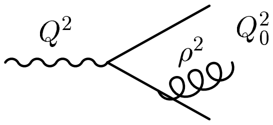

$$\mathbf{\Delta}_{S_3}(Q^2,\rho^2,Q_0^2) \approx \prod_{i=1}^{4} \Delta_i(\rho_i^2) = \Delta_q(Q^2,Q_0^2)\frac{\Delta_q(Q^2,Q_0^2)}{\Delta_q(\rho^2,Q_0^2)}\Delta_q(\rho^2,Q_0^2)\Delta_g(\rho^2,Q_0^2) = \left[\Delta_q(Q^2,Q_0^2)\right]^2 \Delta_g(\rho^2,Q_0^2)$$

Figure 6: Structure of the Sudakov form factor for a 3-parton event. Q^2 is the initial scale of the process, ρ^2 an intermediate branching scale and Q_0^2 the final scale. Approximately, the probability for a quark or antiquark to evolve between Q^2 and ρ^2 is given by $\frac{\Delta_q(Q^2,Q_0^2)}{\Delta_q(\rho^2,Q_0^2)}$.

where i runs so all intermediate and final partons in the state are associated to a corresponding Δ_q or Δ_g, e.g. as illustrated in **figure 6** for a 3-parton state.

Parton shower n-jet rates are written as a product of the branching probabilities for $(n-2)$ emissions, given by eq. (8), together with the probabilities for no branching occurring at earlier stages, given by the Sudakov form factors of eq. (11). We obtain

$$\begin{aligned}
R_2(Q^2,Q_0^2) &= \mathbf{\Delta}_{S_2}(Q^2,Q_0^2) \\
R_3(Q^2,Q_0^2) &= \int_{Q_0^2}^{Q^2} d\rho^2\ \alpha_s(\rho^2) c_{1,1}^{PS}(\rho^2)\mathbf{\Delta}_{S_3}(Q^2,\rho^2,Q_0^2) \\
R_4(Q^2,Q_0^2) &= \int_{Q_0^2}^{Q^2} d\rho^2 \int_{Q_0^2}^{\rho^2} d\rho'^2\ \alpha_s(\rho^2)\ \alpha_s(\rho'^2)\ c_{2,2}^{PS}(\rho^2,\rho'^2)\mathbf{\Delta}_{S_4}(Q^2,\rho^2,\rho'^2,Q_0^2),
\end{aligned} \tag{12}$$

where the coefficients $c_{n,n}^{PS}$ symbolically represent the contributions from the $(n-2)$ branchings at the relevant intermediate scales.

2.3 Colour-Dipole Cascade Model, CDM

The CDM [13, 14] is a model of parton cascades based on the fact that a gluon, emitted from a $q\bar{q}$-pair in an e^+e^- collision, can be treated as radiation from the colour dipole between the q and the $\bar{q}$, and that to a good approximation, the emission of a second softer gluon can be treated as radiation from two independent dipoles, one between the q and the g and one between the g and the $\bar{q}$. In the CDM this is generalised so that the emission of a third, still softer gluon, is given by the decay of three independent dipoles etc.

Generally two initial particles spanning a dipole, decay into three particles spanning two independent dipoles. The emission is characterised in phase space by transverse momentum and rapidity, $(p_\perp^2, y)$, with

$$p_\perp^2 = \frac{\left(s_{12}-(m_1+m_2)^2\right)\left(s_{23}-(m_2+m_3)^2\right)}{s_{123}} \tag{13}$$

$$y = \frac{1}{2}\ln\left(\frac{s_{12}-(m_1+m_2)^2}{s_{23}-(m_2+m_3)^2}\right). \tag{14}$$

Parton 2 being the emitted one, $x_i = 2\frac{E_i}{\sqrt{s}}$ the energy fraction carried by parton i in the rest frame of the mother dipole, and $s_{i,j,\ldots} = (p_i+p_j+\ldots)^2$ the invariant mass squared of a system, see **figure 7** for an illustration.

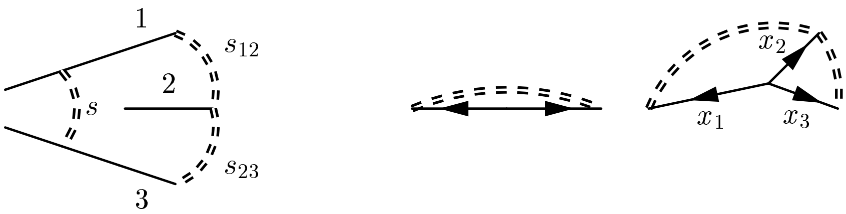

Figure 7: **Left:** Colour dipole between parton 1 and 3 with dipole mass s_{123} radiates parton 2 so that two new independent dipoles are formed. **Right:** Dipole splitting in the rest frame of the mother dipole.

We can rewrite the measure for the $2 \to 3$ phase space in eq. (2), as $d\Omega_{i\to f} = \left(\prod_{f=1}^{3} \frac{d\mathbf{p}_f}{(2\pi)^3 2E_f}\right) \times (2\pi)^4 \, \delta^4 \left(\sum_{i=1}^{2} p_i - \sum_{f=1}^{3} p_f\right)$, so that the cross section can be expressed as

$$\sigma_{i\to f} = \frac{1}{8\,(2\pi)^5\, s} \int |\mathcal{M}_{i\to f}|^2 dp_\perp^2 dy = \frac{1}{8\,(2\pi)^5\, s} \int |\mathcal{M}_{i\to f}|^2 dx_1 dx_3. \tag{15}$$

We introduce three possible splittings functions for the radiation of gluons through decays of dipoles, $q\bar{q} \to qg\bar{q}$, $qg(\bar{q}g) \to qgg(\bar{q}gg)$, $gg \to ggg$, as [14]

$$\frac{d\sigma_{q\bar{q}\to qg\bar{q}}}{dx_1 dx_3} = \frac{2\alpha_s}{3\pi} \frac{x_1^2 + x_3^2}{(1-x_1)(1-x_3)} \tag{16}$$

$$\frac{d\sigma_{qg\to qgg}}{dx_1 dx_3} = \frac{3\alpha_s}{4\pi} \frac{x_1^2 + x_3^3}{(1-x_1)(1-x_3)} \tag{17}$$

$$\frac{d\sigma_{gg\to ggg}}{dx_1 dx_3} = \frac{3\alpha_s}{4\pi} \frac{x_1^3 + x_3^3}{(1-x_1)(1-x_3)}. \tag{18}$$

Gluons are taken massless and partons are always kept *on-shell* throughout the evolution in ARIADNE. When splitting a dipole, both partons connected to it receive energy through the distribution of recoils (see [1]). In the limit of validity for the LLA and parton showers, i.e. *strong ordering* in $p_\perp^2$, the emissions factorize and the CDM correctly reproduces the Altarelli-Parisi equations.

2.3.1 Gluon splitting

When a gluon has been emitted, there is a competition between emitting further gluons from one of its two dipoles, or splitting it into a secondary $Q\bar{Q}$-pair. This competition is controlled by means of the ordering of emissions and the Sudakov form factors. In ARIADNE secondary pair production is favoured more than in other standard parton showers.

The splitting of gluons into *secondary* quark-antiquark pairs, $Q\bar{Q}$, is incorporated into the CDM through the approximate factorization of the full $q\bar{q}Q\bar{Q}$ matrix element, as $\sigma_{q\bar{q}\to q\bar{q}Q\bar{Q}} \approx \sigma_{q\bar{q}\to qg\bar{q}} \times \sigma_{qg\bar{q}\to q\bar{q}Q\bar{Q}}$, valid in the limit of small invariant mass of the produced $Q\bar{Q}$-pairs.

Since the CDM treats dipoles, the gluon splitting, $\sigma_{qg\bar{q}\to q\bar{q}Q\bar{Q}}$, is not uniquely associated to either of the two dipoles connected to it, but rather receives contributions from both. The default procedure in ARIADNE is to simply assign half of the gluon splitting probability to each of the dipoles, i.e. $\sigma_{qg\bar{q}\to q\bar{q}Q\bar{Q}} = \sigma_{qg\to qQ\bar{Q}} + \sigma_{g\bar{q}\to\bar{q}Q\bar{Q}}$. In this manner a qg dipole has the splitting function [19]

$$\frac{d\sigma_{qg\to qQ\bar{Q}}}{dx_1 dx_3} = \frac{1}{2} \cdot \frac{\alpha_s}{4\pi} \frac{(1-x_2)^2 + (1-x_3)^2}{1-x_1}, \tag{19}$$

which in the limit $x_1 \to 1$ ($x_2 \to z$ and $x_3 \to (1-z)$), becomes half of the $P_{g\to q\bar{q}}$ in eq. (7).

If a *collinear* gluon is emitted by a *primary* quark in the CDM, the invariant mass of the quark-gluon dipole produced, s_{qg}, is small and should not contain enough energy to split the gluon into a massive $Q\bar{Q}$-pair.

Since $\sigma_{qg\bar{q}\to q\bar{q}Q\bar{Q}}$ also is associated with the large $g\bar{q}$-dipole, the collinear gluon may split into a $Q\bar{Q}$-pair anyway. It is unreasonable that the gluon collinear to the quark, should contribute with half of the splitting probability, and through recoil distributions take energy from the distant antiquark. We can instead associate the splitting to a probability proportional to the inverse mass squared of the connecting dipoles.

We use this reasoning to make an alternative, uneven division of the gluon splitting function, associating a fraction, $\frac{1/s_{qg}}{(1/s_{qg}+1/s_{g\bar{q}})}$, with the collinear gq-dipole

$$\frac{d\sigma_{qg\to qQ\bar{Q}}}{dx_1 dx_3} = \frac{\frac{1}{s_{qg}}}{\frac{1}{s_{qg}} + \frac{1}{s_{g\bar{q}}}} \cdot \frac{\alpha_s}{4\pi} \frac{(1-x_2)^2 + (1-x_3)^2}{1-x_1}, \tag{20}$$

and the rest to the $g\bar{q}$-dipole. This should reduce the peculiar situations when soft and/or collinear gluons are split into massive $Q\bar{Q}$-pairs.

2.4 Jet clustering

In general one may describe the clustering algorithms as the reconstruction of QCD cascades backwards in time.

Characteristic for the different studies of jet structures in e^+e^- annihilations performed over the years is the introduction of a resolution or distance parameter, and its use to systematically group or *cluster* adjacent objects into jets[11].

Most of these algorithms use a binary clustering scheme, where the number of final particles is successively reduced when joining the two *closest* objects found into one, their energy and momenta are redistributed according to some *recombination* scheme[12]. Objects remaining after the execution of the algorithm are the jets of the event, with a lower boundary for their *separation* given by the resolution parameter.

- The JADE algorithm [21] originally set the standard for binary clustering schemes, it suggested the choice of resolution based on invariant mass, y_{cut}. A test variable is computed for all tentative reconstructions of parton pairs

  $$y_{ij} = \frac{2E_i E_j\,(1-\cos\theta_{ij})}{E_{vis}^2} \quad \text{with} \quad E_{vis}^2 = (E_{CM} - E_{undetected})^2\,, \tag{21}$$

  and the smallest value found is compared to a resolution parameter y_{cut}. If $y_{ij} < y_{cut}$ the i and j are recombined into one object. The algorithm is executed and the recombinations performed as long as any $y_{ij} < y_{cut}$ are found.

- It was eventually understood that the soft gluon emissions do not exponentiate, as in eq. (4), when ordered in invariant mass, while they do when ordered in transverse momentum [16]. The $k_\perp$-clustering or DURHAM algorithm [22] introduced a somewhat

[11] See [20] for a review.

[12] Among possible recombination schemes we mention: The simple addition of the four-momenta into a massive object. The addition of three-momenta into a massless objects. And the addition of the four-momenta, keeping the total energy and direction fixed, into massless objects.

more sophisticated choice of resolution, based instead on transverse momenta. The test variable became

$$y_{ij} = \frac{2\left(1-\cos\theta_{ij}\right)\min\left\{E_i^2, E_j^2\right\}}{E_{vis}^2}. \tag{22}$$

The smallest y_{ij} found is compared with the cutoff y_{cut}. If $y_{ij} < y_{cut}$ the i and j are recombined into one object. The algorithm is executed as long as any $y_{ij} < y_{cut}$ are found.

- For the CDM, it was convenient to introduce a new scheme, more suitable to the $2 \to 3$ branchings of the dipole cascade. The DICLUS algorithm [23, 20] uses a resolution based on transverse momentum, $p_{\perp cut}^2$, and repetitively recombines $3 \to 2$ objects[13]. Test variables are computed for all possible reconstructions for an object i with respect to two other objects j and k

$$p_{\perp ijk}^2 = \frac{s_{ij}s_{jk}}{s_{ijk}}. \tag{23}$$

The smallest value found is compared with the resolution. If $p_{\perp ijk}^2 < p_{\perp cut}^2$ the energy and momenta of the three objects is redistributed among two *massless* objects. The algorithm is executed as long as any $p_{\perp ijk}^2 < p_{\perp cut}^2$ are found.

The jet rates found by the algorithms vary with the resolution parameter, $R_n\left(y_{cut}\right)$ or $R_n\left(p_{\perp cut}^2\right)$, s o the number of jets observed may differ at different resolutions. The sum of jet rates should remain constant, $\sum_n R_n = 1$.

3 Combining matrix elements with the CDM

The CDM already uses first order matrix elements for its first emission, although not taking quark masses completely into account. We will here improve it, by incorporating fully massive tree-level matrix elements to order α_s^{n-2}.

For this study, we will use the number of outgoing partons $n = 4$, as given by the COMPHEP program [24] when regulated by a resolution cutoff in invariant mass, Q_{cut}^2.

We will allow the generated 2-, 3- or 4-parton states from COMPHEP to enter a QCD cascade, modelled by the CDM in ARIADNE, until a lower limit for the perturbative approach is reached, given as a resolution cutoff in transverse momentum, $p_{\perp cut}^2$.

The generations of partons is divided in two stages:

1. An n-parton state (with hard emissions correctly reproduced) is selected according to its corresponding cross section, $\frac{\sigma_{i\to f}}{\sum_f \sigma_{i\to f}}$, given by matrix element calculations. Also given are a set of momenta for the outgoing partons and their colour connections, e.g. see **figure 8**.
2. The evolution of the n-parton state is continued, interfacing the information from the above stage with the CDM cascade, i.e. correcting the n-parton state with a Sudakov form factor and with the running of the coupling, and allowing a dipole shower to populate the soft and collinear regions. We carefully consider the phase space entering in the Sudakov corrections. The many-parton structure achieved is needed for the resummation of higher orders to be valid, and for the applicability of hadronization models.

[13] There are ambiguities on how to perform the $3 \to 2$ recombinations, we refer the reader to [12] for a complete discussion.

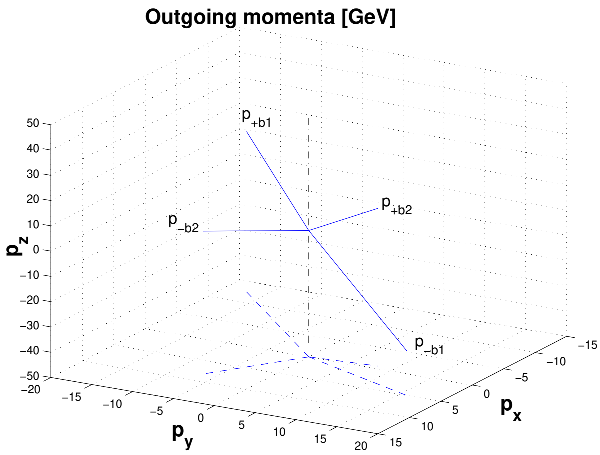

Figure 8: Matrix element generated $e^+e^- \to b_1\bar{b}_1b_2\bar{b}_2$ state. Outgoing momenta is shown, with the prefix '+' indicating a quark, and '−' an antiquark. The cross section for the process is 10 pb, and the colour connections are between partons ($+b1$,$-b1$) and ($+b2$,$-b2$)

An outline of the algorithm used here to match the matrix elements with the CDM will be presented in **section 3.3**.

3.1 Reconstruction of emissions

Before correcting the n-parton state with the Sudakov form factor, we will need to *reconstruct* the scales of branchings that would have occurred if the n-parton state had been produced by the primary $q\bar{q}$-pair entering the CDM directly.

From the momenta of the n partons, given by the matrix element generator, e.g. $p_{+b1}, p_{-b1}, p_{+b2}$ and p_{-b2} in **figure 8**, the scales for the tentative CDM branchings can be successively reconstructed, using a modified version of the Diclus clustering algorithm discussed in **section 2.4**. The reconstructions need to be consistent with ordering in transverse momentum and colour charges.

A particular n-parton event, with splittings corresponding to the reconstructed scales, might be reached through several shower histories. When selecting which one to enter the cascade, we will follow the procedure proposed in [25], i.e. to weight all possible shower histories with their respective splitting probabilities, and randomly choose one among these.

In rare cases, where no *ordered* dipole history can be found, the reconstructions are modified so that when one of the *unordered* histories is chosen, and a reconstructed branching scale is found at some value smaller than another corresponding to a subsequent branching, the larger scale is chosen for both; i.e. if from a $qgg\bar{q}$ state, the $q\bar{q} \to qg\bar{q}$ branching is found at a smaller $p_\perp^2$ than the $qg\bar{q} \to qgg\bar{q}$, then the larger $p_\perp^2$ is chosen for both branchings in the reconstruction.

The matrix elements are also corrected for the running of the coupling, by rejecting events with probability

$$\frac{1}{\alpha_{s0}^{n-2}} \prod_{i=1}^{n-2} \alpha_s(p_{\perp i}^2), \tag{24}$$

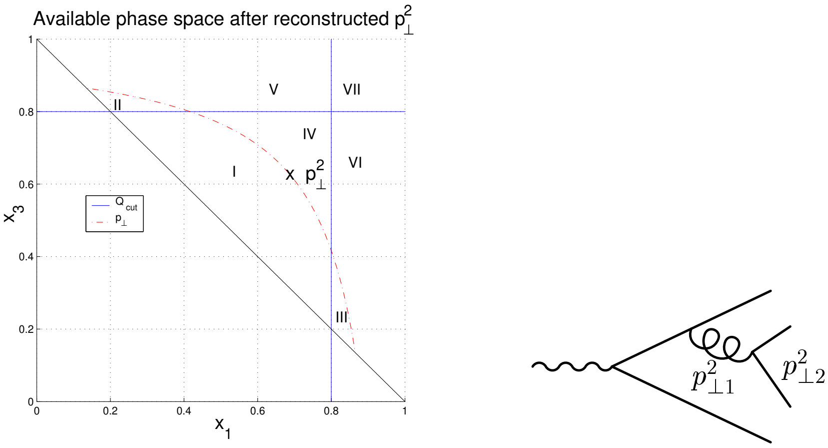

Figure 9: Illustration of the phase space available for emissions. From a matrix element reconstructed 4-parton state, we obtain two ordered branching scales in transverse momenta, $p_{\perp 1}^2 \geq p_{\perp 2}^2$. Regions I-III above illustrate the phase space entering the Sudakov form factor to an intermediate state associated with some reconstructed $p_\perp^2$.

where α_{s0} is a constant value for the strong coupling, used throughout the generation of the matrix elements[14], and $p_{\perp i}^2$ are the reconstructed branching scales.

3.2 Sudakov veto algorithm

The n-jet ratios for the Sudakov corrected matrix elements are given by

$$\begin{aligned}
R_2(Q^2, Q_{cut}^2) &= \mathbf{\Delta}_{S_2}^{PS}\left(Q^2, Q_{cut}^2\right) \\
R_3(Q^2, Q_{cut}^2) &= \alpha_{s0} \int_{Q_{cut}^2}^{Q^2} d\rho^2 \; c_{1,1}^{ME}(\rho^2) \mathbf{\Delta}_{S_3}(Q^2, \rho^2, Q_{cut}^2) \\
R_{4+}(Q^2, Q_{cut}^2) &= \alpha_{s0}^2 \int_{Q_{cut}^2}^{Q^2} d\rho^2 \int_{Q_{cut}^2}^{\rho^2} d\rho'^2 \; c_{2,2}^{ME}(\rho^2, \rho'^2) \mathbf{\Delta}_{S_3}(Q^2, \rho^2, \rho'^2).
\end{aligned} \tag{25}$$

where α_{s0} is constant, $c_{n,n}$ the *unintegrated* versions of the $C_{n,n}$ previously introduced in eq. (3), and the 4+ subscript is explained later on in this section.

The Sudakov form factors to an n-parton state, $\mathbf{\Delta}_{S_n}$, can be obtained when regarded as the no-emission probability into specific regions of the phase space available. We give an illustration of the phase space entering the sudakov when the emissions are ordered in $p_\perp^2$ in **figure 9**, considering:

1. The relation $x_2 = 2 - x_1 - x_3$ gives a kinematical constrain for the emissions, e.g. for massless partons, a diagonal $x_1 + x_3 > 1$ in the $x_1 x_3$-plane.
2. A cutoff in invariant mass within the matrix elements gives, through $s_{ij} = s_{ijk}\,(1 - x_k)$, upper limits for x_3 and x_1 respectively, above which no emissions can be generated.
3. A branching scale in transverse momentum, reconstructed from some matrix element generated state gives, through $p_{\perp ijk}^2 = s_{ijk}\,(1 - x_i)\,(1 - x_k)$, a restriction for emissions ordered in $p_\perp^2$, as outgoing hyperbolas in the $x_1 x_3$-plane.

[14] To ensure an acceptance value below 1, α_{s0} must be larger than any other α_s. It is therefore taken at the parton shower cutoff, $p_{\perp cut}^2$.

We effectively obtain $\mathbf{\Delta}_{S_n}$ by repetitively rejecting the n-parton states, whenever trial emissions from the reconstructed intermediate states are associated to the regions I-III described above, i.e. whenever these emissions are found to correspond to higher branching scales, or earlier stages of the evolution, than the ones reconstructed from the matrix elements.

When applying the Sudakov form factor to a state of highest order in α_s, 4-parton states in this study, we would rather have an expression for the 4-or-higher jet rate, R_{4+}. Therefore we do not correct with the Sudakov factor after the highest order intermediate state has been accepted, and allow the jet-structure to be altered before reaching Q^2_{cut}.

We then have, for a 4-parton reconstructed state two ordered emissions, $p^2_{\perp 1} \geq p^2_{\perp 2}$, and proceed as:

- A higher reconstructed scale, $p^2_{\perp 1}$, will exclude events where trial emissions started at Q^2 are found to be generated at higher branching scales, $p^2_{\perp} > p^2_{\perp 1}$, i.e. if the trial emission falls in region I-III in **figure 9**, the event is rejected.
- A lower reconstructed scale, e.g. $p^2_{\perp 2}$, should as above exclude events where trial emissions, started at $p^2_{\perp 1}$, are found to generate branchings with $p^2_{\perp} > p^2_{\perp 2}$, but since we rather have a R_{4+} ratio in eq. (25) we allow all emissions once the intermediate 3-parton state above has been accepted.

The procedure outlined in this section corresponds exactly to weighting the matrix element generated n-parton states with its respective Sudakov form factor. Allowing these corrected states to continue in the CDM, we force the two hardest emissions to fit the exact tree-level matrix elements, as long as they are inside the region of phase space covered by the matrix element generation.

3.3 Matching algorithm

The algorithm used for the matching of matrix element and parton showers is outlined as follows:

1. First the number of partons, $n \leq N$, and flavours, are chosen and generated with $\mathcal{O}(\alpha_s^{n-2})$ tree-level matrix elements, according to $\frac{\sigma_{i\to f}}{\sum_f \sigma_{i\to f}}$, i.e. tree-level contributions to the rates $R_n\left(Q^2, Q^2_{cut}\right)$ in eq. (3). The invariant $p^2_{\perp}$'s of the n partons is checked, and if anyone is below $p^2_{\perp cut}$, the state is rejected and the procedure is restarted.
2. All the intermediate states $S_2, \ldots, S_{n-1}$ and intermediate scales $p^2_{\perp 1}, \ldots, p^2_{\perp n-2}$ corresponding to a sequence of ordered dipole emissions are reconstructed according to the algorithm in **section 3.1**.
3. The generated state is adjusted to the running of the coupling, when kept with a probability given by equation (24). If it is rejected, we restart at step 1.
4. We now make a trial emission with the dipole cascade from the state S_2, starting from the maximum scale limited by the centre of mass energy. If this emission is at a scale above $p^2_{\perp 1}$, the whole event is rejected and we restart from step 1.
5. If the S_2 state was accepted, a trial emission is performed from the state S_3, with a maximum scale $p^2_{\perp 1}$. If this trial emission is at a scale above $p^2_{\perp 2}$, the event is rejected and we restart from step 1. This procedure is repeated for all states down to S_{n-1}. If no rejection has been made, a trial emission is made from the matrix element generated n parton state starting from the scale $p^2_{\perp n-2}$. There are now two cases:
   (a) If $n = N$, the event is accepted, the trial emissions are always kept, and the cascade is allowed to continue down to the cutoff $p^2_{\perp cut}$.
   (b) If $n < N$, and all parton pairs possible after the last trial emission are above the matrix element cutoff, $s_{ij} > Q^2_{cut}$, the event is rejected and we restart from step 1. If any of the pairs is found below, $s_{ij} < Q^2_{cut}$, this emission is accepted and the

cascade continued, down to the cutoff $p^2_{\perp cut}$.

4 Results

For the sake of simplicity (c.f. **figure 4**), $e^+e^- \xrightarrow{\gamma^*} n$-parton contributions are excluded from our calculations, and we only keep track of the dominant Z^0-channel at LEP energies, where $E_{CM} = m_{Z^0} = 91.2\, GeV$.

The combined procedure described in this report has been tested using massless partons [12], we have chosen for this report to make use of the default quark masses of the CompHEP program, given as $m_u = m_d = 0$, $m_s = 0.2\ GeV$, $m_c = 1.42\ GeV$, and $m_b = 4.62\ GeV$. In [12], the *dependence* on Q^2_{cut} was found to be small. Here we will use $Q_{cut} = 9\ GeV$, at which the jet rate weights become $R_2 : R_3 : R_4 \approx 27.4 : 50.3 : 22.3$, as Q_{cut} is lowered, the right hand side weights increase.

The cutoff in transverse momentum used in the dipole cascade is $p_{\perp cut} = 0.6\ GeV$. At this scale, using the same $\Lambda_{QCD} = 0.22\ GeV$ as in Ariadne, the strong coupling becomes $\alpha_{s0} = 0.12201$.

4.1 Event shapes

In order to confirm that our interface with the CompHEP program is working properly, we look at standard *global* event shapes which are known to be well reproduced by the event generators.

For each event, we look at the distribution of the **thrust**, which is defined as

$$T\left(p_1^\mu, \ldots, p_n^\mu\right) = \max_{|\bar{\mathbf{n}}|=1} \frac{\sum_{i=1}^n |\bar{\mathbf{p}} \cdot \bar{\mathbf{n}}|}{\sum_{i=1}^n |\bar{\mathbf{p}}|} \tag{26}$$

and quantifies how pencil-shaped an event is. $\bar{\mathbf{n}}$ is taken to be the direction with greatest momentum flow.

The **thrust** is sensitive to massive quarks, in the sense that the decaying heavy *mesons* will obtain a large $p_\perp$ with respect to the jets, and the momentum flow along these directions will be large, furthermore, a suppressed radiation of gluons from heavy quarks leads to events where T is closer to 1.

We plot this distribution in **figure 10** and find that the CompHEP interface to Ariadne, here referred to as MEPS, are close, as is expected if there are no serious errors in the implementations or discrepancies between the approaches. We note that a vast majority of the events are in the region $0 < 1 - T < 0.2$, i.e. configurations where jets are found close to each other.

4.2 Particle production

Statistics on rejected matrix element generated states containing heavy quark-antiquark pairs, and also the cross sections for this combined approach, are given in **table 1**.

We see that the efficiency is low. This is expected since our corrections for the Sudakov form factors, and the running of the coupling, force a crude rejection of a great deal of

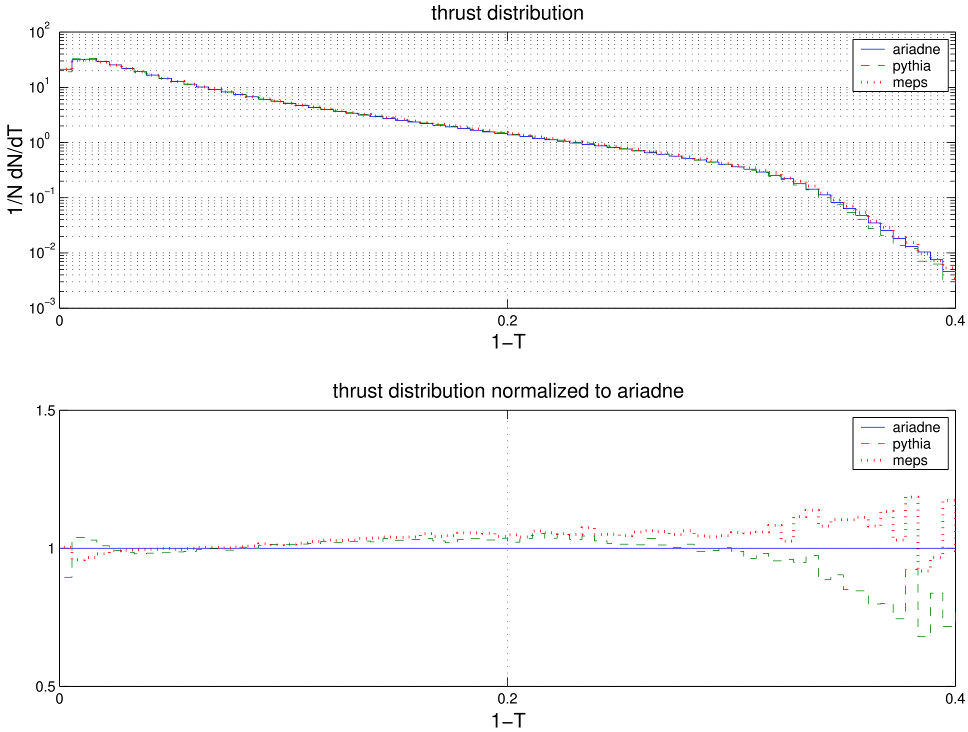

Figure 10: Distribution of thrust with respect to all partons from events generated by Ariadne, Pythia and MEPS.

events. This efficiency is expected to decrease even further if Q_{cut} is lowered.

4.2.1 Secondary $B\bar{B}$-production

In parton showers, all intermediate decays and the colour flow in the cascade are available through a recorded shower history. We know that the ordering of emissions also, in some sense, is an ordering in time, i.e. earlier emissions are generated at greater scales than subsequent ones.

In the matrix elements, as when reconstructing decay vertices from particle trajectories recorded at experiments, it makes no sense to speak of a quark-antiquark pairs being *secondary* or emitted from any particular source.

State	Accepted [%]	σ_{meps} [pb]	State	Accepted [%]	σ_{meps} [pb]
$c\bar{c}$	28.2	2032	$b\bar{b}$	21.2	1941
$cg\bar{c}$	10.6	3616	$bg\bar{b}$	10.6	5040
$cgg\bar{c}$	4.0	1494	$bgg\bar{b}$	4.2	2222
$u\bar{u}c\bar{c}$	5.2	36	$u\bar{u}b\bar{b}$	5.1	49
$d\bar{d}c\bar{c}$	5.1	47	$d\bar{d}b\bar{b}$	5.1	47
$s\bar{s}c\bar{c}$	5.1	47	$s\bar{s}b\bar{b}$	5.2	47
$c\bar{c}c\bar{c}$	5.1	17	$c\bar{c}b\bar{b}$	5.2	51
$b\bar{b}c\bar{c}$	5.2	51	$b\bar{b}b\bar{b}$	5.1	21

Table 1: Statistics on rejected matrix elements and cross sections in our approach.

	Ariadne [%]	Ariadne [%]	Pythia [%]	Herwig [%]	MEPS [%]	MEPS [%]
opt		new $g \to Q\bar{Q}$				new $g \to Q\bar{Q}$
$C\bar{C}$	2.47	1.65	1.17		2.57	1.76
$B\bar{B}$	0.36	0.20	0.14	0.25	0.39	0.30
$c\bar{c}c\bar{c}$	0.45	0.30	0.20		0.45	0.31
$c\bar{c}b\bar{b}$	0.51	0.34	0.27		0.56	0.40
$b\bar{b}b\bar{b}$	0.076	0.034	0.034		0.078	0.062

	Delphi [%]	Aleph [%]	Sld [%]	Delphi [%]
$B\bar{B}$	$0.21 \pm 0.11 \pm 0.09$	$0.277 \pm 0.042 \pm 0.057$	$0.307 \pm 0.071 \pm 0.066$	$0.33 \pm 0.10 \pm 0.04$

Table 2: **Up:** Rate of events containing at least *one* heavy secondary $Q\bar{Q}$-pair, or at least *two* heavy pairs. **Down:** Experimental data for gluon splittings to secondary $B\bar{B}$-pairs. The rightmost column contains data from the Delphi experiment, reconstructed from $b\bar{b}b\bar{b}$ observables, whereas the rest are reconstructed from secondary $b\bar{b}$ signals in 4-jet samples, see [11].

When we look for *massive* $q\bar{q}$- or $Q\bar{Q}$-pairs in our approach, we need to explicitly specify a criterion to determine which pair in the event we should consider to be the primary one. We have chosen to consider the pair with highest invariant mass, as primary to other pairs of lower invariant mass.

Experimental data indicates a larger production of secondary $B\bar{B}$-pairs than is predicted by other standard parton shower models. Ariadne has a ratio of $Q\bar{Q}$-pair production which is higher, and rather overestimates the production of secondary $Q\bar{Q}$-pairs.

We have introduced a new splitting function for the gluons in eq. (20), and are interested in the new results we might obtain from this.

In **table 2** we present the fraction of events where secondary heavy $Q\bar{Q}$-pairs were found, also experimental results for gluon splittings into secondary $B\bar{B}$-pairs are presented.

We see that the matrix element corrected approach, MEPS, gives an even higher $Q\bar{Q}$-pair production rate than the standard Ariadne, due to the increased number of hard emission higher order matrix elements imply.

The uncertainties in the experimental data are still too big to draw strong conclusions on a true $Q\bar{Q}$-pair production rate. Nevertheless, we are confident in the arguments presented in support of eq. (20), and we notice a reduced $Q\bar{Q}$-pair production for both Ariadne and MEPS when this new splitting function is used, although still larger than in Pythia and Herwig, and in reasonable agreement with data.

Studying the distribution of secondary heavy quarks in rapidity, **figure 11**, we do not see much difference between Ariadne and MEPS.

We have argued that $g \to Q\bar{Q}$ splittings are controlled by the ordering of the emissions and by the Sudakov form factors. On the matrix elements, we impose the same ordering as in Ariadne through the reconstruction of branching scales. This means that the partons emitted from MEPS are not expected be distributed in regions of phase space noticeably distant from the standard Ariadne distributions. The difference with Pythia is larger, indicating again that the choice of ordering is important when populating the available phase space.

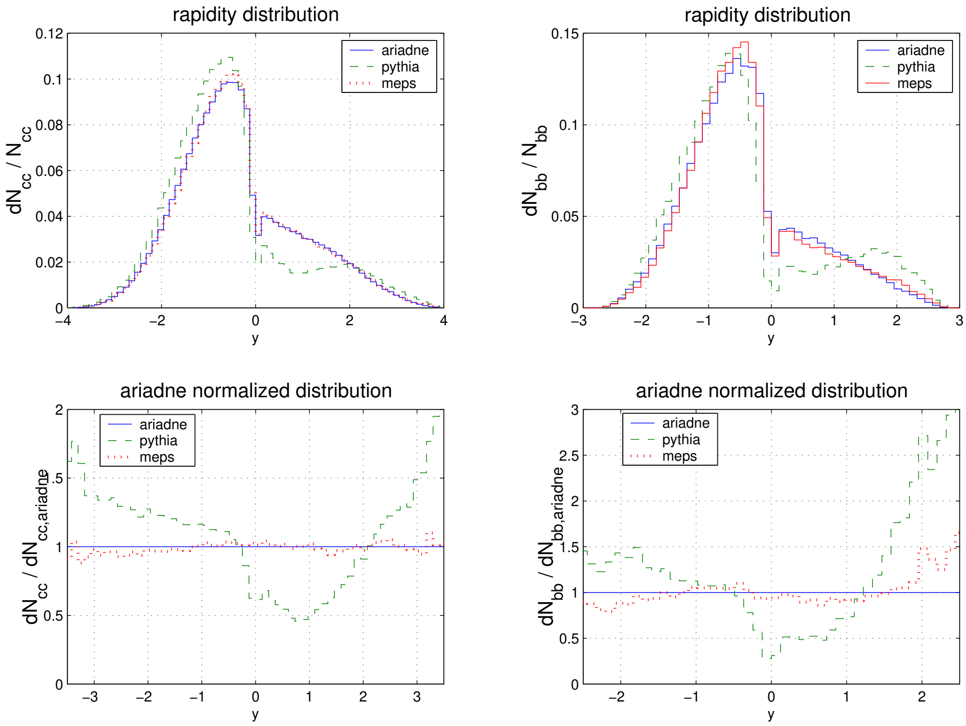

Figure 11: Rapidity distributions for secondary quarks and antiquarks, produced by ARIADNE, PYTHIA and MEPS are compared.

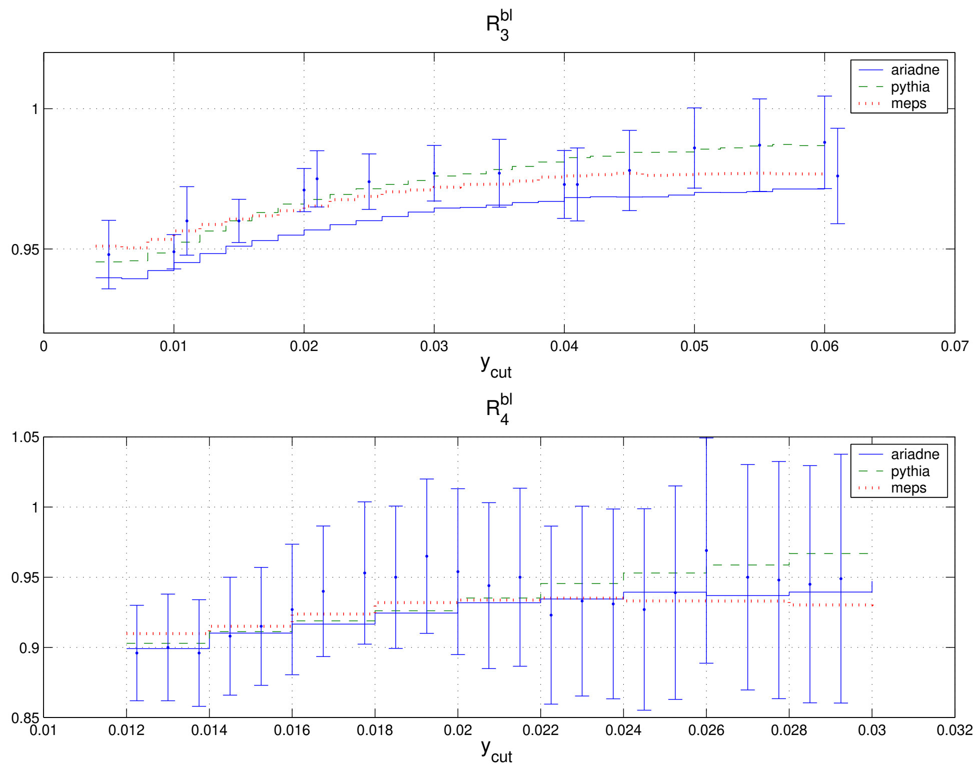

Figure 12: Jet rates, R_3^{bl} and R_4^{bl}, using the DURHAM-clustering algorithm, are presented for Ariadne, Pythia and MEPS.

4.3 Jet rates

One observable sensitive to QCD effects of heavy quarks is the ratio of n-jet rates, between events found to contain primary $b\bar{b}$-pairs and events found to contain *light* primary *uds* quark-antiquark pairs

$$\mathcal{R}_n^{bl}(y_{cut}) = \frac{R_n^b(y_{cut})}{R_n^l(y_{cut})}. \tag{27}$$

$\mathcal{R}_n^{bl}$ can be interpreted as a measure of the suppression of gluon radiation off quarks due to their mass. A better understanding of R_n^{bl} leads to an increased understanding of mass effects in parton cascades, and a more precise determination of the b-quark mass.

It was found in [11] that ARIADNE underestimated the R_3^{bl} ratio. PYTHIA did better after making modifications to the splitting functions for heavy quarks [26]. New results for MEPS are presented in **figure 12**.

We find that the new procedure does increase R_3^{bl} to a satisfactory level. Also R_4^{bl} is increased for $y_{cut} < 0.02$, which is a change in the right direction, but the statistical errors in the data as well as Monte Carlo uncertainties are here much larger, and it is difficult to draw strong conclusions.

The data has been corrected for hadronization in a model-dependent way, but we conclude that the new results give a good indication of better agreement with data. To reduce uncertainties, hadronization should be incorporated to the predictions from event generators and comparisons should be performed directly with hadron level measurements.

5 Conclusions and outlook

A working interface for *massive* higher order matrix elements corrections to ARIADNE is presented, and a global event shape, **thrust**, is shown to be in agreement with standard distributions. The new interface increases perturbative secondary heavy $Q\bar{Q}$-pair production, and significantly improves the reproduction of the ratio R_3^{bl} previously underestimated by ARIADNE. Statistical errors need to be reduced before stronger conclusions can be made.

In general, further investigations are needed to draw stronger conclusions on the true secondary $B\bar{B}$-pair production, i.e. both in the experimental data and in the modelling, which depends strongly on the ordering used in the cascade and in the reconstruction of branchings. We believe that if the order of the matrix elements is increased, e.g. $\mathcal{O}\left(\alpha_s^3\right)$, this dependence will be reduced.

The incorporation of matrix elements into the CDM needs to be improved, as it is presently too cumbersome and too inefficient to be used in a standard fashion.

In addition, it would be desirable to extend the treatment to ep and pp collisions.

Acknowledgments

I would like to thank Leif Lönnblad, Stephen Burby, Gösta Gustafson and Torbjörn Sjöstrand. Thank you! thank you! thank you! thank you!.

References

[1] Leif Lönnblad. *Comput. Phys. Comm.*, 71:15, 1992.

[2] T. Sjöstrand, P. Edén, C. Friberg, L. Lönnblad, G. Miu, S. Mrenna, and E. Norrbin. *Computer physics communication*, 135:238, 2001.

[3] G. Corcella, I. Knowles, G. Marchesini, S. Moretti, K. Odagiri, P. Richardson, M. Seymour, and B. Webber. *hep-ph/0107071*, 2001.

[4] Particle data group of LBNL. The particle adventure. *http://particleadventure.org*, 2000.

[5] CTEQ collaboration. Handbook of perturbative qcd. *http://www.phys.psu.edu/~cteq/*, 2001.

[6] R.K. Ellis, W.J. Stirling, and B.R. Webber. *QCD and collider physics*. Cambridge university press, 1996.

[7] Y. Dokshitzer, V. Khoze, A. Mueller, and S. Troyan. *Basics of perturbative QCD*. Editions frontieres, 1991.

[8] B. Andersson, G. Gustafson, G. Ingelman, and T. Sjöstrand. *Phys. Rep.*, 97:31, 1983.

[9] B. Webber. *Nucl. Phys. B*, 238:492, 1984.

[10] K. Hamacher and M. Weierstall. *hep-ex/9511011*, 1995.

[11] A. Ballestero et.al. Report of the qcd working group. *hep-ph/0006259*, 2000.

[12] Leif Lönnblad. *hep-ph/0112284*, 2001.

[13] G. Gustafson. *Phys. Lett. B*, 175:453, 1986.

[14] G. Gustafson and U. Pettersson. *Nucl. Phys. B*, 306:746, 1988.

[15] R. K. Ellis, D. A. Ross, and A. E. Terrano. *Nucl. Phys. B*, 178:421, 1981.

[16] N. Brown and W.J. Stirling. *Physics Letter B*, 252:657, 1990.

[17] G. Altarelli and G. Parisi. *Nucl. Phys. B*, 126:298, 1977.

[18] V. V. Sudakov. *Sov. Phys. JETP*, 30:65, 1956.

[19] Bo Andersson, Gösta Gustafson, and Leif Lönnblad. *Nucl. Phys B*, 339:393, 1990.

[20] S. Moretti, L. Lönnblad, and T. Sjöstrand. *JHEP*, 08:1, 1998.

[21] W. Bartel et. al. JADE Collaboration. *Z. Phys. C*, 33:23, 1986.

[22] S. Catani, Y. Dokshitzer, M. Olsson, G. Turnock, and B.R. Webber. *Phys. Lett. B*, 269:432, 1991.

[23] Leif Lönnblad. *Z. Phys. C*, 58:471, 1993.

[24] A. Pukhov, E. Boos, M. Dubinin, V. Edneral, V. Ilyin, D. Kovalenko, A. Kryukov, V. Savrin, S. Shichanin, and A.Semenov. Comphep version 41.10. *http://theory.sinp.msu.ru/comphep*, 2000.

[25] J. André and T. Sjöstrand. *Phys. Rev. D*, 57:5767, 1998.

[26] E. Norrbin and T. Sjöstrand. *Nucl. Phys. B*, 603:297, 2001.